Journal of Power Sources 240 (2013) 442–447

Contents lists available at SciVerse ScienceDirect

Journal of Power Sources

journal homepage: www.elsevier.com/locate/jpowsour

Pd doped Co_3O_4 nanowire array as the H_2O_2 electroreduction catalyst

Kui Cheng, Fan Yang, Yang Xu, Lin Cheng, Yanyan Bao, Dianxue Cao, Guiling Wang*

Key Laboratory of Superlight Material and Surface Technology of Ministry of Education, College of Material Science and Chemical Engineering, Harbin Engineering University, Harbin 150001, China

HIGHLIGHTS

- Pd@Co_3O_4/Ti is prepared via a template-free growth followed by electrodeposition.
- Pd@Co_3O_4/Ti electrode exhibits a current density of 145.8 mA cm^{-2} at −0.4 V.
- The introduction of Pd greatly improves the catalytic activity of Co_3O_4 nanowires.

ARTICLE INFO

Article history:
Received 2 February 2013
Received in revised form
8 April 2013
Accepted 11 April 2013
Available online 19 April 2013

Keywords:
Palladium
Cobaltosic oxide
Nanowire arrays
Electrocatalyst
Hydrogen peroxide reduction

ABSTRACT

Co_3O_4 nanowire arrays freely standing on Ti foil (Co_3O_4/Ti) are prepared via a template-free growth method. Pd nanoparticles are electrochemically deposited by cyclic voltammetry method on Co_3O_4 nanowires to obtain a nanocomposite electrode (Pd@Co_3O_4/Ti). The morphology and phase structure of the Pd@Co_3O_4/Ti electrode are characterized by scanning electron microscope and X-ray diffraction spectrometer. The catalytic activity of H_2O_2 electroreduction on the Pd@Co_3O_4/Ti electrode in alkaline medium is evaluated by means of linear scan voltammetry and chronoamperometry. The Pd@Co_3O_4/Ti electrode exhibits high performance and good stability to H_2O_2 electroreduction with a current density of 145.8 mA cm^{-2} at −0.4 V in 3.0 mol dm^{-3} KOH and 0.4 mol dm^{-3} H_2O_2 electrolyte, which outperforms the bare Co_3O_4 nanowire arrays without Pd doping.

1. Introduction

Hydrogen peroxide (H_2O_2) has been investigated as the oxidant to replace oxygen for liquid-based fuel cells, such as metal semi-fuel cells (MSFCs) [1–6] and direct borohydride fuel cells (DBFCs) [7–12]. These fuel cells were developed as underwater or space power sources working in air-free environments. Compared to oxygen, H_2O_2 has the following advantages when used as oxidant in fuel cells. Firstly, H_2O_2 is in liquid form, which is easier for the fuel cell design, assembly and operation. Secondly, H_2O_2 has faster reduction kinetics than oxygen and also has none of the environmental problems associated with most of other chemical oxidizers. The electrochemical reduction rate of H_2O_2 at the cathode catalysts has great impact on the performance of fuel cells [13–15]. So the study on electrocatalyst for H_2O_2 reduction has brought attention in recent years in the fuel cell community.

Several types of electrocatalysts have been investigated, which include: (1) noble metals, such as platinum, palladium, iridium, gold, silver and a combination of these [1,2,7,12,16–18]; (2) macrocycle complexes of transition metals, such as Fe–and Co–porphyrin, Cu–triazine complexes [19–21]; (3) transition metal oxides, such as cobalt oxides [21–23], ferric oxides [24], manganese [25]. Among these catalysts, noble metals demonstrated better overall performance in terms of high catalytic activity, but the high prices restricted their extensive utilization. In general, the traditional electrode for fuel cells is commonly carbon-supported catalyst powder electrodes made by the traditional slurry-coating technique, that is, the powders are mixed with conducting carbons and polymer binders to form pastes, and then applied to a carbon paper current collector. Such obtained electrodes usually suffer drawbacks of low catalyst utilization because some catalysts are unable to contact with the current collector or are inaccessible to the electrolyte. Therefore, the reduction of noble metals and the superior electrode structure are attracting much attention. In fact, H_2O_2 is not stable in the solution with the decomposition reaction, and the decomposition has fast kinetics in basic medium ($E^0 = 0.878$ V) than in acid medium ($E^0 = 1.776$ V), which reduces

* Corresponding author. Tel./fax: +86 010 451 82589036.
E-mail address: wangguiling@hrbeu.edu.cn (G. Wang).

0378-7753/$ – see front matter © 2013 Elsevier B.V. All rights reserved.
http://dx.doi.org/10.1016/j.jpowsour.2013.04.057

the utilization efficiency of H_2O_2. So the electrode for H_2O_2 electroreduction should have an open 3D structure, ensuring the full utilization of catalyst and allowing the gas bubbles produced by H_2O_2 decomposition diffuse away from the surface of electrode. Therefore, more attention has been paid to the preparation of the composites between noble metals and other catalytic materials. Examples are Pt–CuO [26], Au–ZnO [27] which can further enhance the performance of catalyst and also improve the efficiency of noble metals.

Currently, the hybrid structure of nanoparticle-decorated nanowire arrays (NP@NW) combines the high aspect ratio and highly controllable structure of an oriented nanowire skeleton with the large surface area of nanoparticles [28]. The fabrication of decorating arrays of NWs with NPs includes many methods such as general sol-flame [28], thermal growth [29,30], electrochemical deposition [31] and so on. Among them, electrodeposition is a simple, scalable, and controllable manner. Various morphologies and sizes can be easily prepared by changing the electrochemical parameters. Based on the above considerations, we presently aim to develop the synthesis of nanocomposite with nanowire arrays as the skeleton for deposition of noble metal nanoparticles. Co_3O_4 is commonly used as the electrocatalyst for H_2O_2 reduction, however, it has low electric conductivity and catalytic performance. Many reports [32–34] have revealed that Co_3O_4 decorated with metal particles could increase the conductivity and further improve the performance. Pd as one of noble metal electrocatalyst has been demonstrated high catalytic activity and good stability for H_2O_2 electroreduction [14,15,35]. In this paper, we successfully prepared a novel three-dimensional (3D) nanocomposite electrode ($Pd@Co_3O_4$/Ti) through two-step strategy that the compact Co_3O_4 nanowire arrays were firstly growth on Ti foil by template-free growth followed by the electrodeposition of Pd nanoparticles on them. The effect of the electrodeposition condition of Pd on the electrochemical performance has been systematically investigated. The catalytic performance for H_2O_2 electroreduction on $Pd@Co_3O_4$/Ti electrode was also examined.

2. Experimental

2.1. Preparation and characterization of $Pd@Co_3O_4$/Ti electrode

The schematic illustration of the experimental setup is shown in Fig. 1. The preparation process mainly involves two steps. In the first step, Ti foil supported Co_3O_4 nanowire arrays was prepared via a template-free growth method [36]. Briefly, a growth solution was prepared by dissolving 10 mmol $Co(NO_3)_2$ and 5 mmol NH_4NO_3 into a solution consisting of 35 mL H_2O and 15 mL ammonia (30 wt %). The solution was magnetically stirred for 10 min in air at room temperature and then heated at 90 °C for 2 h (reaction solution). Ti foils ($10 \times 10 \times 0.25$ mm^3) were degreased ultrasonically in acetone, isopropanol and ethanol sequentially, followed by polishing in a solution containing H_2O, HF and HNO_3 with a volume ratio of 5:1:4 for 1 min to remove the surface oxide layer, and then rinsed with water extensively. The Ti foil was immersed in the reaction solution, and the solution was heated for 12 h at 90 °C for nanowire arrays growth. The obtained nanowire arrays were washed with H_2O, and calcined at 300 °C for 2 h in air. In the second step, Pd was deposited on Co_3O_4/Ti substrate via cyclic voltammetry electrodeposition in a solution containing $PdCl_2$ and 0.1 mol dm^{-3} KCl (the supporting electrolyte). The pH value of the solution was controlled at 9.5. The Co_3O_4/Ti was dipped into this solution. The electrodeposition was performed by cyclic voltammetry (CV) in the potential rage of −0.2 ∼ −0.8 V. X-ray powder diffraction (XRD) patterns of the catalysts were recorded with a Rigaku TTR III with Cu K radiation ($\lambda = 0.1514178$ nm). The 2θ scan range is from 10° to 80° with a scan rate of 5 min^{-1} and a step width of 0.01°. The surface morphology was examined by JSM-6480 scanning electron microscope (SEM) equipped with energy dispersive X-ray spectrometer (EDX).

2.2. Electrochemical measurements

The electrochemical experiments were carried out in a typical three-electrode glass electrochemical cell using a computerized potentiostat (Autolab PGSTAT302, EcoChemie). The $Pd@Co_3O_4$/Ti electrode acted as the working electrode, a saturated Ag/AgCl, KCl electrode served as the reference electrode and a glassy carbon rod behind a D-porosity glass frit was employed as the counter electrode (eliminating the influence of H_2O_2 hydrolysis). All potentials were referred to the reference electrode. All electrochemical measurements were performed at room temperature. The electrolyte was 3.0 mol dm^{-3} aqueous KOH solution. All solutions were made with analytical grade chemical reagents and Millipore Milli-Q water (18 MΩ cm). Electrochemical impedance measurements were performed by applying an AC voltage with 5 mV amplitude in a frequency range from 0.01 Hz to 100 kHz.

3. Results and discussion

3.1. Determination of the electrodeposition conditions for Pd deposition on Co_3O_4 nanowire arrays by cyclic voltammetry method

In order to determine the optimal electrochemical parameters for the deposition of Pd on the surface of nanowire arrays by cyclic voltammetry method, polarization curves under various different conditions were recorded in Fig. 2. The potential ranged from −0.2 V to −0.8 V to ensure Pd easily deposited on surface of Co_3O_4 nanowire arrays. Fig. 2A shows the influence of different concentration of $PdCl_2$ during the electrodeposition progress. The electrodeposition cycles are preliminary set at 5 with the

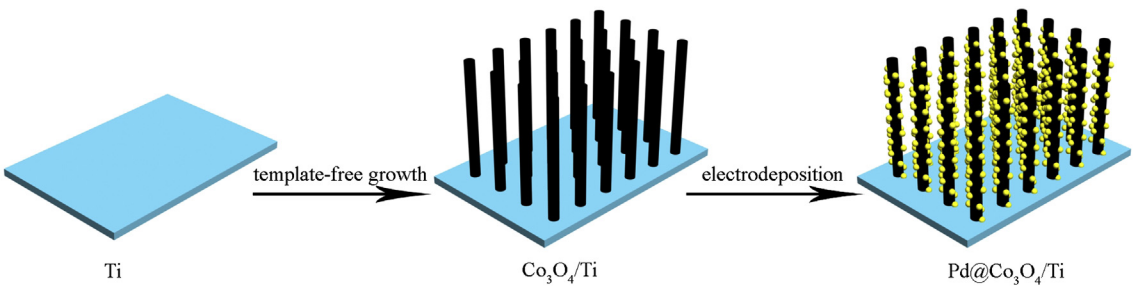

Fig. 1. Schematic diagram of the formation of Co_3O_4 nanowire arrays and $Pd@Co_3O_4$/Ti electrode.

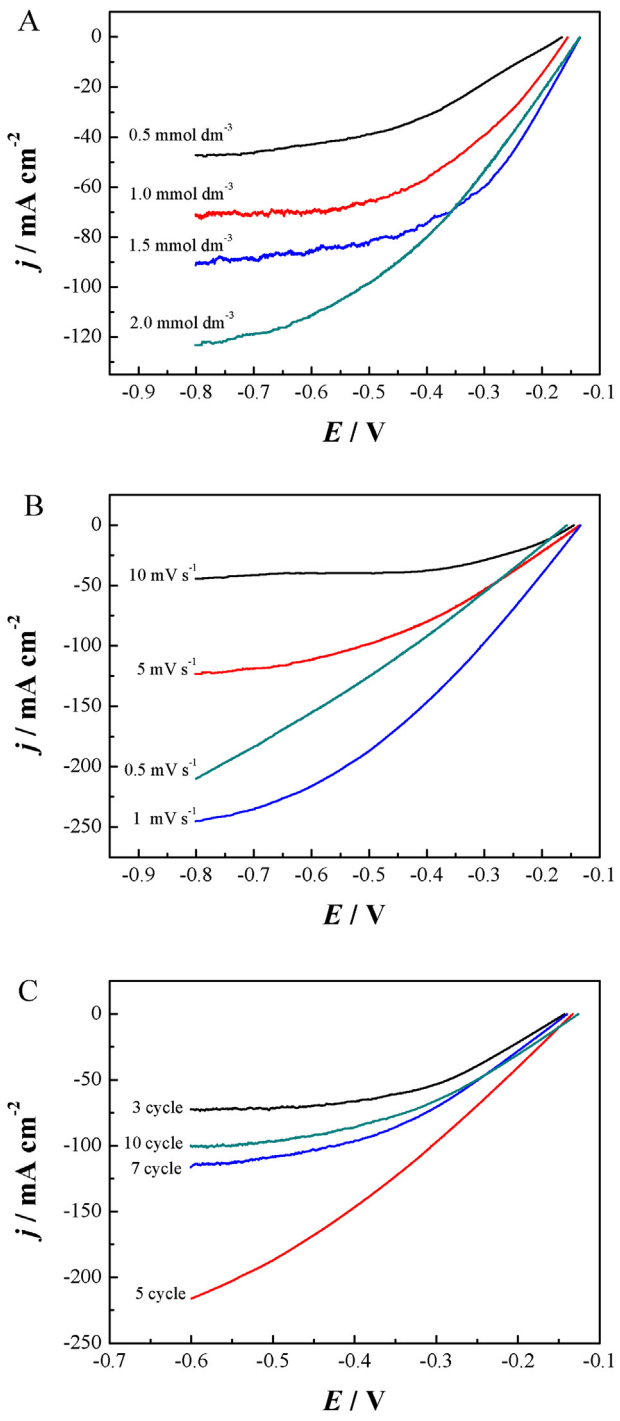

Fig. 2. (A) Comparative polarization curves for H_2O_2 reduction in 0.4 mol dm^{-3} H_2O_2 + 3.0 mol dm^{-3} KOH under different concentration of $PdCl_2$ with the electrodeposition rate of 5 mV s^{-1}. Scan rate: 5 mV s^{-1}. (B) Comparative polarization curves for H_2O_2 reduction in 0.4 mol dm^{-3} H_2O_2 + 3.0 mol dm^{-3} KOH under different electrodeposition scan rate. Scan rate: 5 mV s^{-1}. (C) Comparative polarization curves for H_2O_2 reduction in 0.4 mol dm^{-3} H_2O_2 + 3.0 mol dm^{-3} KOH under different electrodeposition cycles with the electrodeposition rate of 1 mV s^{-1}. Scan rate: 5 mV s^{-1}.

electrodeposition rate of 5 mV s^{-1}. Clearly, the catalytic performance for H_2O_2 reduction on the Pd@Co_3O_4/Ti electrode increased with the increase of $PdCl_2$ concentration in the electroplating liquid. However, the increase was not obvious when $PdCl_2$ concentration was higher than 1.5 mmol dm^{-3}, since that excess Pd deposited on the surface of Co_3O_4 nanowire arrays may be increase the size of Pd to decrease the surface area of Pd. A suitable concentration of Pd^{2+} is beneficial for the improvement of catalytic activity and the high efficiency of Pd, consequently, an electrodeposition solution of 2.0 mmol dm^{-3} $PdCl_2$ + 0.1 mol dm^{-3} KCl is determined in this paper.

Scan rate of cyclic voltammetry method by influencing the speed of the electrodeposition, directly affects the number of Pd depositions, and thus influences the conductivity of the electrode and the contact area of catalyst with electrolyte. Fig. 2B shows the effects of electrodeposition rate on the catalytic activity of Pd@Co_3O_4/Ti electrode. Different scan rates of 0.5 mV s^{-1}, 1 mV s^{-1}, 5 mV s^{-1} and 10 mV s^{-1} were applied during the electrodeposition Pd on Co_3O_4 nanowires with the same electrodeposition cycles of 5. Too high or too low electrodeposition rates could not yield the best catalytic performance for H_2O_2 reduction. When chose 1 mV s^{-1} as the scan rate of electrodeposition, a reduction current density of 145.8 mA cm^{-2} at −0.4 V was successfully achieved, indicating that the catalytic activity was increased by 300% than that of 10 mV s^{-1}.

In fact, an increase or decrease of electrodeposition cycles can remarkably affect the electrodeposition time. During the electrodeposition progress, reasonable control of electrodeposition cycles becomes necessary. Similar to the effect of electrodeposition rate, a suitable electrodeposition cycles are needed. It can be seen from Fig. 2C, the highest catalytic performance can be obtained when electrodeposition cycles controlled is to be 5. In summary, the optimal electrodeposition condition included the solution of 2.0 mmol dm^{-3} $PdCl_2$ + 0.1 mol dm^{-3} KCl, the electrodeposition rate of 1.0 mV s^{-1} and the electrodeposition cycles of 5.

3.2. Characterization of the Pd@Co_3O_4/Ti electrode

Fig. 3 shows the XRD patterns of Co_3O_4 and Pd@Co_3O_4 powder. To eliminate the influence of Ti substrate, we obtained the sample powders by scraping them from Ti foil. As observed in Fig. 3, several well-defined diffraction peaks are observed at 2θ values of 19.0°, 31.1°, 36.8°, 44.8°, 59.3°, 65.1°. All of these peaks can be successfully indexed to (111), (220), (311), (400), (511), and (440) plane reflections of the pure spinel Co_3O_4 (JCPDS card No. 42–1467). Differing from the pattern of Co_3O_4, except the characteristic peak of Co_3O_4, the peaks located at about 41°, 46° and 68° correspond to (111), (200), and (220) of Pd on the Pd@Co_3O_4 (JCPDS card No. 46–1043). It can be concluded that Pd was uniformly electrodeposited on Co_3O_4 nanowire arrays.

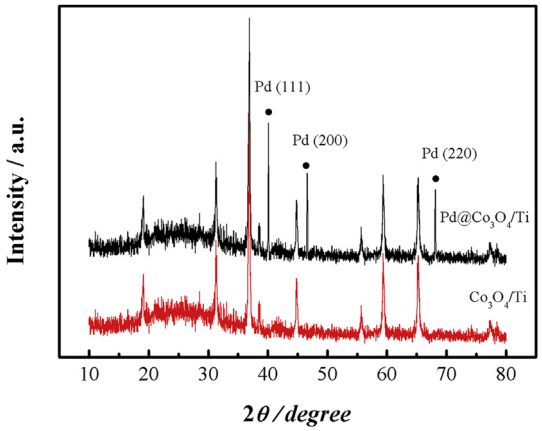

Fig. 3. XRD patterns of Co_3O_4 and Pd@Co_3O_4 powder.

Fig. 4 shows the different-magnification SEM images of Pd@Co_3O_4/Ti electrode and the corresponding EDX spectrum. It can be clearly seen from Fig. 4A that Ti substrate was completely covered by Co_3O_4 nanowire arrays. Ti foil as the substrate for the direct growth of Co_3O_4 nanowire arrays has many advantages, since that Ti is a kind of inert metals which can be steadily existed in the harsh acid or alkaline medium. Besides, the catalyst directly grows on the current collection (Ti foil), and the thickness of Ti foil used in this article is only 0.25 mm, such the ultrathin substrate making the preparation of membrane electrolyte assembly of PEMFC much easier. Conventionally, the MEA is composed of seven layers. The anode and cathode catalyst layers are adhered to the Nafion membrane, the catalyst layer is loaded on a microporous layer of polytetra-fluoroethylene bonded carbon black, which is supported on macroporous carbon paper or cloth [37]. Based on the novel Pd@Co_3O_4/Ti electrode, a novel MEA structure was designed, where the carbon black layer of the traditional diffusion layer was eliminated. This structure of electrode has the better mass transport and the catalyst is not loaded on the surface of the diffusion layer, but is loaded inside the diffusion layer, which also makes the fuel cell more compact and convenient. The nanowire arrays have diameters of around 250 nm, lengths up to around 15 μm (Fig. 4B and C). This open 3D structure provides a superior support framework for the deposition of Pd. Meanwhile, to characterize the chemical composition of the electrode, EDX spectrograms were recorded and analyzed. Specifically, element mapping by EDX is used to record the elemental composition of the surface. The spectrogram of the EDX measurement shows that the characteristic peaks of the metallic Pd and Co (Fig. 4D, the Co element present here is ascribed to the Co_3O_4 nanowire arrays). EDX results demonstrate that the surface of Co_3O_4 nanowire arrays included Pd and the content of Pd element in the Pd@Co_3O_4 is about 1%.

Fig. 5 shows the cyclic voltammograms of Co_3O_4/Ti and Pd@Co_3O_4/Ti electrode in 3.0 mol dm^{-3} KOH solution at a sweep rate of 5 mV s^{-1}. The insert is the cyclic voltammograms of Pd/Ti electrode. The Pd/Ti electrode was prepared by electrodeposition of Pd on Ti foil using the same methods as that of Pd@Co_3O_4/Ti electrode in the solution of 2.0 mmol dm^{-3} $PdCl_2$ + 0.1 mol dm^{-3} KCl, ensuring the same Pd content on the two electrodes. Two strong anodic current peaks, peak A and B, were found for both electrodes. These peaks can be attributed to the oxidation of Co_3O_4 to $Co(OH)_3$ and $Co(OH)_3$ to CoO_2, respectively, according to literatures [36]. The cathodic peaks can be assigned to the reduction of $Co(OH)_3$ to Co_3O_4 (peak A′). The CV profile of Pd@Co_3O_4/Ti electrode is very similar to that of Co_3O_4/Ti except that a new cathodic peak at −0.4 V was observed (peak C′). This additional peak for Pd@Co_3O_4/Ti electrode can be ascribed to the reduction of Pd surface oxides according to literatures [14], demonstrating that Pd was deposited on Co_3O_4. The charge obtained from the cathodic peaks centered at −0.43 V in the CV of Pd/Ti and Pd@Co_3O_4/Ti electrodes were employed to estimate the electrochemically active surface area of Pd assuming that a monolayer of PdO was formed and its reduction charge value is 405 μC cm^{-2} [38]. Such estimated electrochemically active surface area (EASA) is 16.06 cm^2 for Pd/Ti electrode and 97.78 cm^2 for Pd@Co_3O_4/Ti electrode. The EASA of Pd@Co_3O_4/Ti electrode is

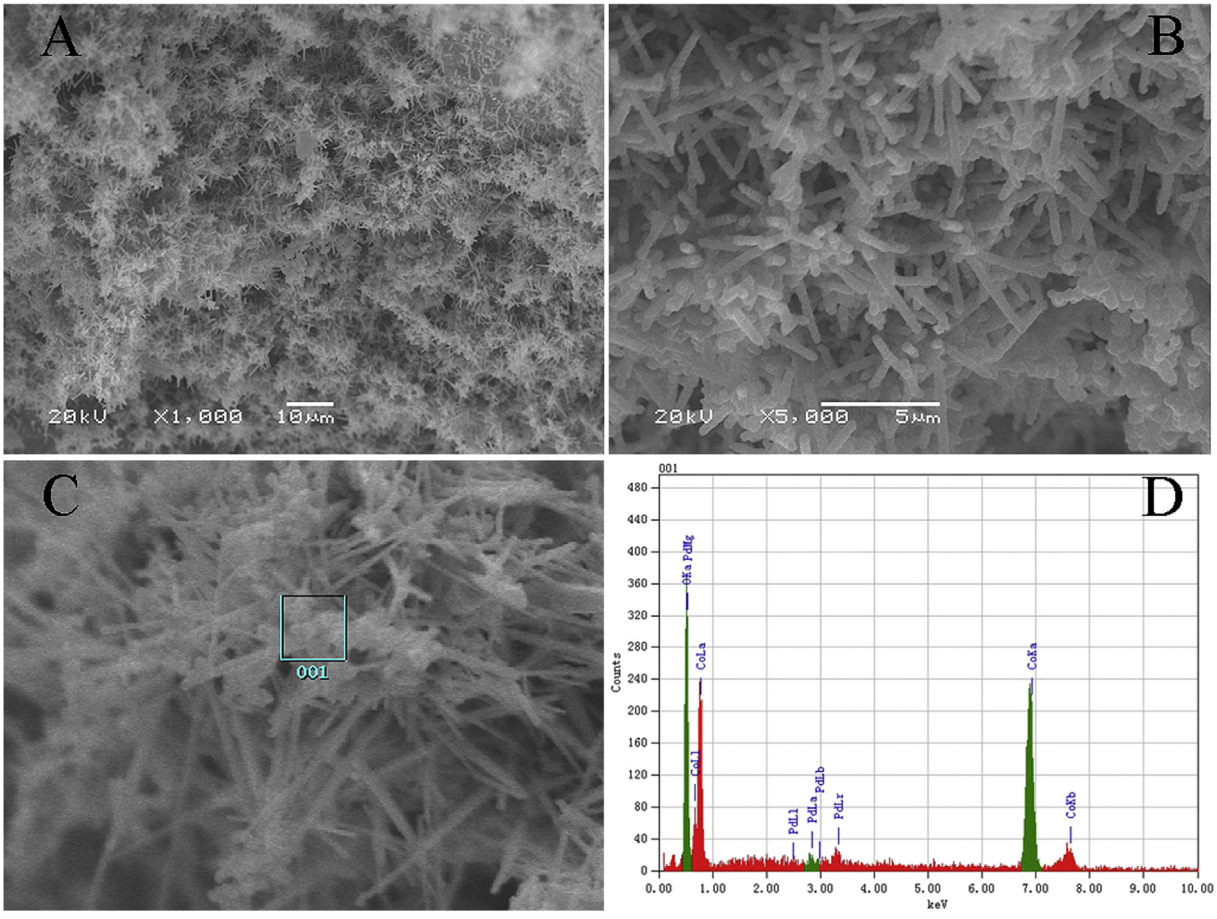

Fig. 4. Different-magnification SEM images of Pd@Co_3O_4/Ti electrode (A, B and C) and the corresponding EDX spectrum (D).

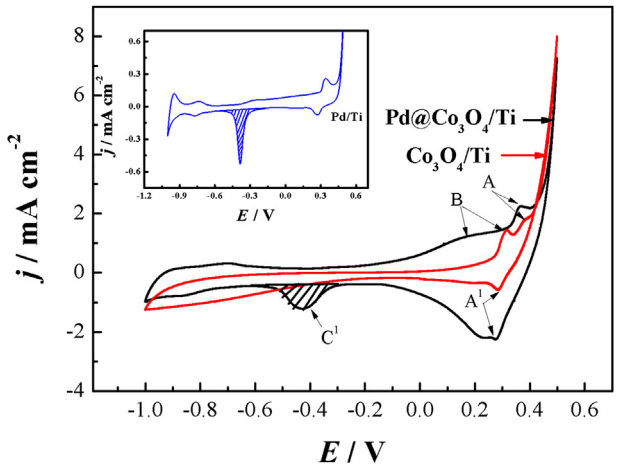

Fig. 5. Cyclic voltammograms of Co_3O_4/Ti and Pd@Co_3O_4/Ti electrode in 3.0 mol dm^{-3} KOH solution. Scan rate: 5 mV s^{-1}. Insert is the cyclic voltammograms of Pd/Ti electrode in 3.0 mol dm^{-3} KOH solution. Scan rate: 5 mV s^{-1}.

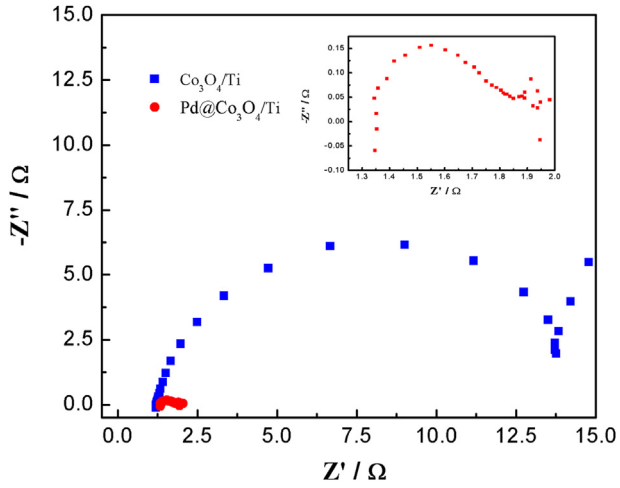

Fig. 7. Electrochemical impedance spectra of the Co_3O_4/Ti and Pd@Co_3O_4/Ti electrode measured in 0.4 mol dm^{-3} H_2O_2 + 3.0 mol dm^{-3} KOH. Inset is the zoom of electrochemical impedance spectra of Pd@Co_3O_4/Ti electrode.

remarkably larger than that of Pd/Ti electrode, which can be attributed to the Co_3O_4 nanowire electrode possesses an open 3D support framework for the deposition of Pd.

3.3. Electrocatalytic performance of the Co_3O_4/Ti and Pd@Co_3O_4/Ti electrode

Fig. 6 shows the performance comparison between Co_3O_4/Ti, Pd/Ti and Pd@Co_3O_4/Ti toward H_2O_2 electroreduction. The insert is the comparative polarization curve of Pd/Ti and Pd@Co_3O_4/Ti electrodes at unit EASA of Pd. The onset reduction potential on the Pd@Co_3O_4/Ti electrode was around −0.13 V, and that on the Pd/Ti and Co_3O_4/Ti shifted to a negative value of 300 mV. At −0.5 V, a high reduction current density of 190 mA cm^{-2} was achieved, in comparison, it can be seen that the catalytic performance for H_2O_2 electroreduction on the Pd/Ti and Co_3O_4/Ti electrode are also much lower than that of Pd@Co_3O_4/Ti electrode. We also compare the catalytic performance of Pd/Ti and Pd@Co_3O_4/Ti electrodes at unit EASA of Pd. It can be observed that Pd@Co_3O_4/Ti electrode exhibits higher catalytic performance towards H_2O_2 electroreduction than Pd/Ti electrode, demonstrating that there were synergistic effects between the Pd and the Co_3O_4 nanowire support. Literatures [32–34] have demonstrated that Co_3O_4 decorated by metal particles are commonly has higher performance and good conductivity. So it can be believed that Pd nanoparticles may play a dual role in this case. On the one hand, the Pd nanoparticles improve the conductivity of the Co_3O_4 nanowires. On the other hand, the metallic Pd could catalyze the electrochemical reduction of H_2O_2 at its surface. In general, Co_3O_4 as the electrocatalyst for H_2O_2 electroreduction has been widely investigated [21,36]. The introduction of Pd could enhance the electrical conductivity of Co_3O_4 and also obtain the synergistic effect between Pd and Co_3O_4 for H_2O_2 electroreduction.

Fig. 7 shows the electrochemical impedance spectra of the Co_3O_4/Ti and Pd@Co_3O_4/Ti electrode measured in 0.4 mol dm^{-3} H_2O_2 + 3.0 mol dm^{-3} KOH. In KOH solution, the spectrum displayed a semicircle at high and low frequency region both on the Co_3O_4/Ti and Pd@Co_3O_4/Ti electrode. Nevertheless, the diameter of Pd@Co_3O_4/Ti electrode was apparently smaller than that of Co_3O_4/Ti electrode, revealing that the charge transfer rate of the Pd@Co_3O_4/Ti electrode is much faster which leads to the higher reduction rate. From Figs. 6 and 7, it can be concluded that the introduction of Pd could remarkably enhance the electrical conductivity of Co_3O_4 and further improve the catalytic performance for H_2O_2 electroreduction.

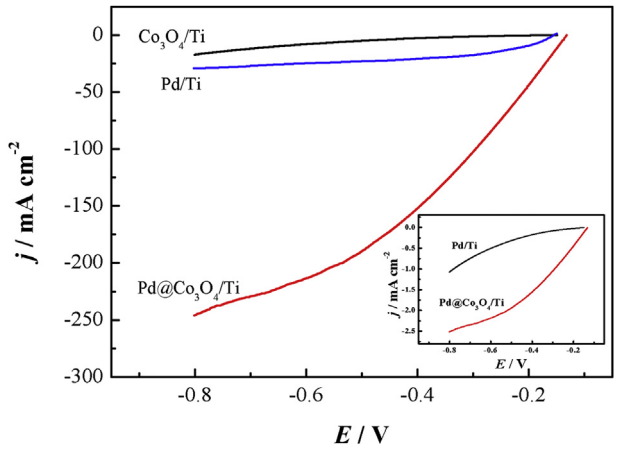

Fig. 6. The comparative catalytic performance of Pd/Ti and Co_3O_4/Ti and Pd@Co_3O_4/Ti electrodes for H_2O_2 reduction in the solution of 0.4 mol dm^{-3} H_2O_2 + 3.0 mol dm^{-3} KOH. Scan rate: 5 mV s^{-1}. Inset is the comparative catalytic performance for H_2O_2 reduction on the Pd/Ti and Co_3O_4/Ti electrodes at unit EASA of Pd. Scan rate: 5 mV s^{-1}.

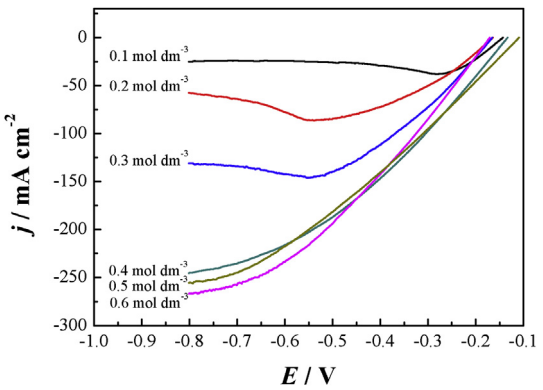

Fig. 8. The effect of H_2O_2 concentration for H_2O_2 reduction on the Pd@Co_3O_4/Ti electrode in *x* mol dm^{-3} H_2O_2 + 3.0 mol dm^{-3} KOH. Scan rate: 5 mV s^{-1}.

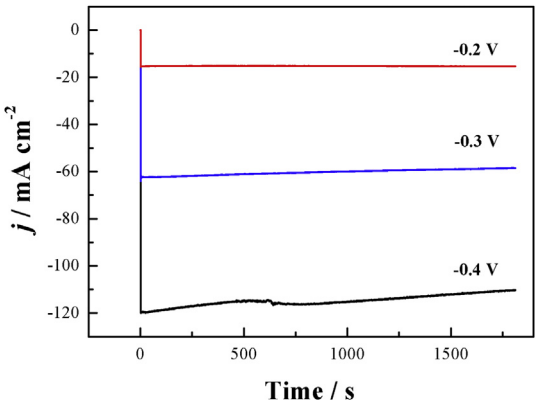

Fig. 9. The chronoamperometric curves for H_2O_2 reduction at different potentials in 3.0 mol dm^{-3} KOH + 0.4 mol dm^{-3} H_2O_2.

Fig. 8 shows the influence of H_2O_2 concentration on the electroreduction performance of for Pd@Co_3O_4/Ti electrode. It can be seen that the cathodic peak current density remarkably increased with the increase of H_2O_2 concentration below 0.4 mol dm^{-3}. The cathodic peak current density displayed an approximate linear relationship with the H_2O_2 concentration, demonstrating that the reduction reaction at the peak potential is controlled by diffusion of H_2O_2. With the increase of hydrogen peroxide concentration, the chemical decomposition of H_2O_2 became significant and the increase of cathodic peak current density was limited. The Pd@Co_3O_4/Ti electrode demonstrated a current density of 145. 8 mA cm^{-2} at −0.4 V, which is higher than Co_3O_4 nanowire grown on nickel foam substrate (90 mA cm^{-2} at −0.4) [36]. This suggests that the Pd@Co_3O_4/Ti electrode has much better catalytic performance than the Co_3O_4 nanowire electrode. The stability of the Pd@Co_3O_4/Ti electrode for H_2O_2 electroreduction at various constant potentials was investigated by chronoamperometric measurements.

Fig. 9 shows chronoamperometric curves for H_2O_2 reduction on the Pd@Co_3O_4/Ti electrode measured in 3.0 mol dm^{-3} KOH containing 0.4 mol dm^{-3} H_2O_2. The current density is nearly constant at −0.2 V, demonstrating that the Pd@Co_3O_4/Ti electrode has a superior stability for H_2O_2 electroreduction. However, the reduction currents slightly decreased with the increase of time at −0.3 and −0.4 V, which is probably due to the decrease of H_2O_2 concentration caused by the high reduction rates at more negative potentials.

4. Conclusions

Spinel Co_3O_4 nanowire arrays on Ti foil substrate are synthesized and then Pd loaded on Co_3O_4 nanowire arrays by an electrochemical deposition method. The Pd doping significantly improved the catalytic performance of Co_3O_4/Ti for H_2O_2 electroreduction and enhanced the electrical conductivity of Co_3O_4. The Pd@Co_3O_4/Ti electrode exhibited a current density of 145.8 mA cm^{-2} at −0.4 V in 3.0 mol dm^{-3} KOH and 0.4 mol dm^{-3} H_2O_2 electrolyte, and also showed good stability. The excellent catalytic performance was ascribed to the unique 3D structure, the high efficiency of Pd and the synergistic effects between the Pd and the Co_3O_4 nanowire support. So the Pd@Co_3O_4/Ti electrode can be a promising candidate for the application in fuel cells.

Acknowledgments

We gratefully acknowledge the financial support of this research by Harbin Science and Technology Innovation Fund for Excellent Academic Leaders (2012RFXXG103), Fundamental Research Funds for the Central Universities (HEUCFT1205) and the Science and Technology Support Program of Jiangsu Province (BE2012152).

References

[1] W. Yang, S. Yang, W. Sun, G. Sun, Q. Xin, J. Power Sources 160 (2006) 1420–1424.
[2] W. Yang, S. Yang, W. Sun, G. Sun, Q. Xin, Electrochim. Acta. 52 (2006) 9–14.
[3] D.J. Brodrecht, J.J. Rusek, Appl. Energy 74 (2003) 113–124.
[4] Ø. Hasvold, K.H. Johansen, O. Mollestad, S. Forseth, N. Størkersen, J. Power Sources 80 (1999) 254–260.
[5] M.G. Medeiros, R.R. Bessette, C.M. Deschenes, C.J. Patrissi, L.G. Carreiro, S.P. Tucker, D.W. Atwater, J. Power Sources 136 (2004) 226–231.
[6] E.G. Dow, R.R. Bessette, G.L. Seeback, C. Marsh-Orndorff, H. Meunier, J. VanZee, M.G. Medeiros, J. Power Sources 65 (1997) 207–212.
[7] G.H. Miley, N. Luo, J. Mather, R. Burton, G. Hawkins, L. Gu, E. Byrd, R. Gimlin, P.J. Shrestha, G. Benavides, J. Laystrom, D. Carroll, J. Power Sources 165 (2007) 509–516.
[8] C.P. de León, F.C. Walsh, A. Rose, J.B. Lakeman, D.J. Browning, R.W. Reeve, J. Power Sources 164 (2007) 441–448.
[9] R.K. Raman, A.K. Shukla, Fuel Cells 7 (2007) 225–231.
[10] R.K. Raman, S.K. Prashant, A.K. Shukla, J. Power Sources 162 (2006) 1073–1076.
[11] N.A. Choudhury, R.K. Raman, S. Sampath, A.K. Shukla, J. Power Sources 143 (2005) 1–8.
[12] L. Gu, N. Luo, G.H. Miley, J. Power Sources 173 (2007) 77–85.
[13] T. Bewer, T. Beckmann, H. Dohle, J. Mergel, D. Stolten, J. Power Sources 125 (2004) 1–9.
[14] F. Yang, K. Cheng, Y. Mo, L. Yu, J. Yin, G. Wang, D. Cao, J. Power Sources 217 (2012) 562–568.
[15] D. Cao, L. Sun, G. Wang, Y. Lv, M. Zhang, J. Electroanal. Chem. 621 (2008) 31–37.
[16] R.R. Bessette, M.G. Medeiros, C.J. Patrissi, C.M. Deschenes, C.N. LaFratta, J. Power Sources 96 (2001) 240–244.
[17] M.G. Medeiros, E.G. Dow, J. Power Sources 80 (1999) 78–82.
[18] H. Liu, L. Zhang, J. Zhang, D. Ghosh, J. Jung, B.W. Downing, E. Whittemore, J. Power Sources 161 (2006) 743–752.
[19] R.K. Raman, A.K. Shukla, J. Appl. Electrochem. 35 (2005) 1157–1161.
[20] V.L.N. Dias, E.N. Fernandes, L.M.S. da Silva, E.P. Marques, J. Zhang, A.L.B. Marques, J. Power Sources 142 (2005) 10–17.
[21] D. Cao, J. Chao, L. Sun, G. Wang, J. Power Sources 179 (2008) 87–91.
[22] B. Lu, D. Cao, P. Wang, G. Wang, Y. Gao, Int. J. Hydrogen Energy 36 (2011) 72–78.
[23] W. Jia, M. Guo, Z. Zheng, T. Yu, E.G. Rodriguez, Y. Wang, Y. Lei, J. Electroanal. Chem. 625 (2009) 27–32.
[24] L. Zhang, Y. Ni, X. Wang, G. Zhao, Talanta 82 (2010) 196–201.
[25] R.X. Feng, H. Dong, Y.D. Wang, X.P. Ai, Y.L. Cao, H.X. Yang, Electrochem. Commun. 7 (2005) 449–452.
[26] X.-M. Miao, R. Yuan, Y.-Q. Chai, Y.-T. Shi, Y.-Y. Yuan, J. Electroanal. Chem. 612 (2008) 157–163.
[27] C. Xiang, Y. Zou, L.-X. Sun, F. Xu, Sens. Actuators. B 136 (2009) 158–162.
[28] Y. Feng, I.S. Cho, P.M. Rao, L. Cai, X. Zheng, Nano Lett. 13 (2012) 855–860.
[29] W. Shi, N. Chopra, J. Nanopart. Res. 13 (2011) 851–868.
[30] Y. Lin, D.W. Baggett, J.-W. Kim, E.J. Siochi, J.W. Connell, ACS Appl. Mater. Interfaces 3 (2011) 1652–1664.
[31] P.L. Taberna, S. Mitra, P. Poizot, P. Simon, J.M. Tarascon, Nat. Mater. 5 (2006) 567–573.
[32] W. Yang, J. Salim, S. Li, C. Sun, L. Chen, J.B. Goodenough, Y. Kim, J. Mater. Chem. 22 (2012) 18902–18907.
[33] Y. Wang, H. Zhou, Chem. Commun. 46 (2010) 6305–6307.
[34] W. Yang, J. Salim, C. Ma, Z. Ma, C. Sun, J. Li, L. Chen, Y. Kim, Electrochem. Commun. 28 (2013) 13–16.
[35] L. Sun, D. Cao, G. Wang, J. Appl. Electrochem. 38 (2008) 1415–1419.
[36] G. Wang, D. Cao, C. Yin, Y. Gao, J. Yin, L. Cheng, Chem. Mater. 21 (2009) 5112–5118.
[37] H. Meng, F. Xie, J. Chen, P.K. Shen, J. Mater. Chem. 21 (2011) 11352–11358.
[38] R. Pattabiraman, Appl. Catal. A 153 (1997) 9–20.